Received: 15 October 2019 | Revised: 14 November 2019 | Accepted: 30 November 2019

DOI: 10.1002/2050-7038.12300

RESEARCH ARTICLE

WILEY

Sliding mode controller-based e-bike charging station for photovoltaic applications

Ruixiang Huang[1] | **Feng Hong**[2,3] | **Davood Ghaderi**[4]

[1]Department of Electrical and Mechanical Technology, Ulanqab Vocational College, Ulanqab, Inner Mongolia Autonomous Region, China

[2]College of Computer and Information, Hefei University of Technology, Hefei, Anhui, China

[3]College of Electrical and Mechanical Engineering, Chizhou University, Chizhou, Anhui, China

[4]Electrical and Electronics Engineering Department of Bursa Technical University, Bursa, Turkey

Correspondence
Feng Hong, College of Computer and Information, Hefei University of Technology, Hefei, Anhui 230601, China.
Email: hgfeng@163.com

Davood Ghaderi, Electrical and Electronics Engineering Department of Bursa Technical University, Bursa, Turkey.
Email: davood.ghaderi@btu.edu.tr

Peer Review
The peer review history for this article is available at https://publons.com/publon/10.1002/2050-7038.12300.

Summary

PV-based and wired type of the electrical bicycles (e-bike) battery charging stations widely is spreading because of the resonant network limitations and low efficiency of the wireless mode for these stations. The generated voltage of many of the PV panels such as JIYANGYIN HR-200 W-24 V at the maximum power point is around 36VDC. So, a step-down converter with a PID controller for Maximum Power Point Tracking (MPPT) of the PV panels is considered between PV panels and boost converter in order to decrease this voltage and enhance the current values for the load side. A sliding mode controller (SMC) equipped with a non-isolated DC-DC boost converter with reduced voltage stresses on the power switch is presented. The step-up converter increases the voltage to the utility level of the e-bike with around 360 Wh amount of energy. The main concerns about the converters are the efficiency, voltage, and current stresses, number of active or passive components in the converter topology and simplicity. In comparison with a conventional step-up converter, the selected converter has a lower dynamic loss in the input inductor that can give a proper efficiency by considering its higher voltage gain. The average state-space model for the SMC is used and the main advantage of the controller is its independency to the inductor current or the amount of the load. The proposed SMC is compared with PID and Fuzzy Logic Controller (FLC) methods and based on the results, the robustness, overshoot, and damping factor of the controller are at an acceptable and better level. All mathematical, simulation and comparison results are presented. A 720 Wh circuit has been implemented for charging all types of the Li-Ion or Li-Polymer batteries with 36VDC and 10 Ah specifications.

KEYWORDS

DC-DC step-up converter, E-bike, electrical charging station (ECS), PV panels, sliding mode controller (SMC)

1 | INTRODUCTION

Energy consumption in the world is constantly increasing. Some traditional energy sources are becoming increasingly depleted and the resulting negativities have started to affect people's quality of life. Either new energy sources should be found or the consumption of used energy sources can be a solution. More than 70% of the European population lives

in urban areas. Factors such as pollution caused by transportation and traffic noise create serious problems for human health. According to research conducted in the USA and Europe, nitrogen oxides and carbon monoxide gases released into the atmosphere have been shown to have great harm to human health.[1] Even the simplest reason, depending on the increasing number of vehicles, leads people to research in order to meet their transportation needs in different ways.

Because of the limited availability of conventional sources and increasing costs, new solutions for transportation have been started. Renewable Energy Sources (RESs) based on electrical energy has become an alternative source in the transportation sector in our era due to its ease of production and cost-effectiveness.[2,3]

We have seen examples of renewable energy applications for vehicle technologies recently. The history of electric vehicles dates back to earlier than for vehicles with internal combustion engines.

The Faraday Laws of the 1830s and the discovery of the DC motor can be considered as the beginning of electric vehicles.[4] The development of electric vehicles continued rapidly until the invention of the internal combustion engine in 1885.[5] As a result of the advantages of electric vehicles alone, electric vehicles continued to be produced and used frequently in the late 1800s and early 1900s.[6-8]

In recent years, electric vehicle technology is completing the movement from research and development units to workshop stages. Now, these organizations have started to design electric vehicles according to the needs of the consumer. There are three different types of electric vehicles (EVs). These are the hybrid, plug-in hybrid and fully electric (battery) vehicles.[9-11] Battery-powered EVs may only use a rechargeable battery as an energy source.

One of the battery-powered electric vehicles is an electric bicycle (E-bike). Some of the aims of using e-bikes are; improving local air quality, reducing noise, reducing greenhouse gas emissions, and facilitating accessibility.[12] E-bike technology is the fastest-growing technology among the electric vehicles introduced to the market.

In an e-bike, the electric motor converts the electrical energy it receives from the accumulator into mechanical energy and provides mobility to the bicycle. As a major obstacle when traveling with a normal bicycle, the duration and distance of the electric bicycle increase due to the fact that it can be lowered to a certain point with the climbing electric bicycle.

To meet the need of batteries in e-bikes, Lithium-ion or lithium polymer batteries are used, because they are lighter and smaller in size.[13-15]

Since the old battery chargers used bridge diodes, the current harmonics were very high. Nowadays, battery chargers are microprocessor controlled and current harmonics have decreased to very low levels. For this purpose, for the wired type of charge stations, a DC-DC boost converter is applied to increase the generated voltage by the PV panel to the desired level of the battery.

Normally, batteries need to be charged through around 36 till 54.5 VDC and since the PV panels normally generate 36 VDC at the maximum power point and 45°C as the nominal operating cell temperature, a boost converter should be used. Other types of batteries with 42, 48, 52 and 54.6 VDC charging voltages can be found in the market.[16,17] So, it will be interesting to design a multi-level charging station by using multi-layer boost converter blocks for all kinds of e-bikes. Different types of this converter have been presented by researches.[18-21]

Although a high ratio transformer is used in the conventional isolated converters such as full-bridge or fly-back converters, the non-isolated type of the converters is preferred based on their lower costs because they do not use the transformer and higher efficiency.[22-24]

The current type isolated converters such as active clamp and full-bridge active clamp step-up converters can receive to higher efficiency and DC voltage gains.[25,26] The initial and primary startup of these converters should be done by more attention and furthermore the total cost of these converters is high because of the number of the power elements, current sensors, and feedback controllers.

So, in order to gain higher efficiency and lower cost of the system, the non-isolated types are suggested. Because of the great parasitic capacitors in the PV panel's ground point, the leakage current of the PV connected non-isolated network is an important issue.[27,28] PWM control algorithms and topologies on the converter side can be used in order to decrease this current. Multi-level boost converters have suggested to reduce the voltage stresses on the power switch and generate the higher DC voltages.[29-31] The Electromagnetic Interface (EMI) and switching losses can be decreased in these converters.[32] The main problem of these topologies is the hard switching specification of the power components and reverse recovery problem of the output diode.

Soft switching techniques including the zero voltage switching (ZVT),[33] zero current switching (ZCS),[34] zero voltage transition (ZVT),[35] and zero current transition (ZCT),[36] are presented to reduce the voltage and current stresses on the power switch or power diodes. But we should consider that many of these techniques use an auxiliary switch that needs

an extra controller for switching purposes that results in more complexity of the structure and the number of the components are increasing in these approaches.

Coupled inductors DC-DC converters also are presented.[36] Also, a combination of these converters with the fly-back converter has been suggested in different studies. But the leakage current and higher number of power switches problems are remaining for these studies.

Reference 37 presents a coupled inductor boost converter with three power switch, four power diodes, two coupled inductors, three capacitors and[38] suggests a configuration with two power switches, one power diode, two coupled inductors, and two capacitors. Higher numbers of coupled inductors and power diodes have been presented in Reference 39 with four diodes, four coupled inductors, and three capacitors by fly-back topology. As can be seen, the switching method and controller design for these configurations really are complex and problems with leakage currents and coupled inductors remain. On the other hand, although these converters can present a high DC gain, but are not suitable for battery charge purposes for an e-bike station. Based on the intrinsic nonlinearity specification of a boost converter, the control process of this converter is difficult. On the other hand, a proper control method should guarantee a fixed DC voltage at the output ends of the converter against the changes in input voltage or output side's load's values. Different kinds of controllers have been suggested for this converter. The classic PI and PID controllers,[40,41] Fuzzy Logic Controllers (FLCs),[42,43] model predictive controllers (MPCs),[44] current mode controllers (CMCs)[45,46] and the sliding mode controllers (SMCs)[47-50] are the main suggested models for these purposes.

Some of these techniques like the FLC and MPC do not need mathematical behavior of the converter and are simple and cheap to be applied. In these methods, the controller gives sample voltages of the output side and compares with the reference voltage and based on the difference between measured and reference voltages, applies a pulse with different duty cycles to fix the output voltage.

Although these techniques are simple in practice, FLC needs many of the fuzzy rules and grades for more accuracy.[42,48] Also, this controller has a low speed and needs for a long time to run. The number of the input variables is limited and there are difficulties in order to determine the membership function parameters and fuzzy rules correctly. The MPC is expensive to be installed and an accurate model of the system is needed to be controlled by this controller.[47-49]

The classic PI and PID controllers make the system have the overshoots and undershoots for a long time and sometimes the damping time of the system is not at an acceptable level.[42-50] Furthermore, the amplitude of the output signals at the sudden changes in input voltage or output loads moments with these overshoots and undershoots values are not desired. These controllers need a detailed and accurate mathematical model of the converter and do not advise for the non-linear topologies with uncertain data.

The performance of these controllers is limited and the P, I and D coefficients of the controller sometimes are difficult to be identified as far as the wrong value of for example P, can make instability for all the system. In the CMC technique, we need to sense the current of the switch and inductor accurately which means more components and losses.

In the simplest way normally a resistor or current transformer is applied, but the resistance technique is not sensitive enough and the current transformer is an expensive component. Furthermore, for higher duty cycles, this method acts instability and for the solution, we will need compensating ramp that can have more complexity. Against all the presented controllers, the SMC is a non-linear based controller that can have a variable structure based on the switching specifications.[49]

This technique is independent of the constraints and has a high-speed dynamic reaction against the disturbances. The main reason that can provide this specification in SMC is its property of acting on all of the variables of the system simultaneously.[50] Despite all its advantages, SMC has disadvantages such as depending on the variable switching frequency, input inductor's current and/or output loads.

Variable switching frequency decreases the performance of the controller and makes more noises and needs complex and bulky filters. The problem will be more serious when the controller depends on current measurements.[47-50]

This study presents a PV based e-bike charging station with an improved boost converter. The control of the boost converter will be done by a SMC technology. The performance of the SMC will be analyzed at the connection times of more batteries.

The average state-space approach SMC is presented to fix to output voltage based on the adjustable sliding surfaces under the fixed switching frequency. The proposed method does not need to give samples of the output load values or input voltage level or current of the inductor or power switch and only needs to measure the instant output voltage.

A buck converter is applied between the PV panel and boost converter in order to enhance the current level and decrease the voltage in input points of the boost converter to can supply the current of the loads. Since in our

implementation the JIYANGYIN HR-200W-24V type of PV panels are applied, at the MPP situation, around 36 VDC can be produced, but since these PV panels are generating different values of power and voltages in different times of a day and based on their structures, the Buck converter block can guarantee a fixed 18VDC on that's output ends for the boost converter. This decrement in voltage value can increase the current level for the boost blocks that is an essential issue for charging stations that need high levels of currents for faster-charging purposes. The topology can be extended to a multi-layer configuration to generate different levels of the voltages for other types of e-bike batteries. As mentioned previously, there are different types of batteries that need different charging voltages like 36, 42, 48 and 52 VDC. So, the proposed configuration can be applied in a multi-layer topology, by this detail that every block can generate different voltages and per block can have several outputs ends to connect more than one e-bike at the same time.

2 | PROPOSED DESIGN

A sample of the charging station is presented in Figure 1A. Figure 1B,C shows different states of the converter. Various configurations can be considered for the proposed converter by different charging strategies. The proposed topology can be applied in only one layer to generate only one level of the output voltage and based on the power of the PV side, the

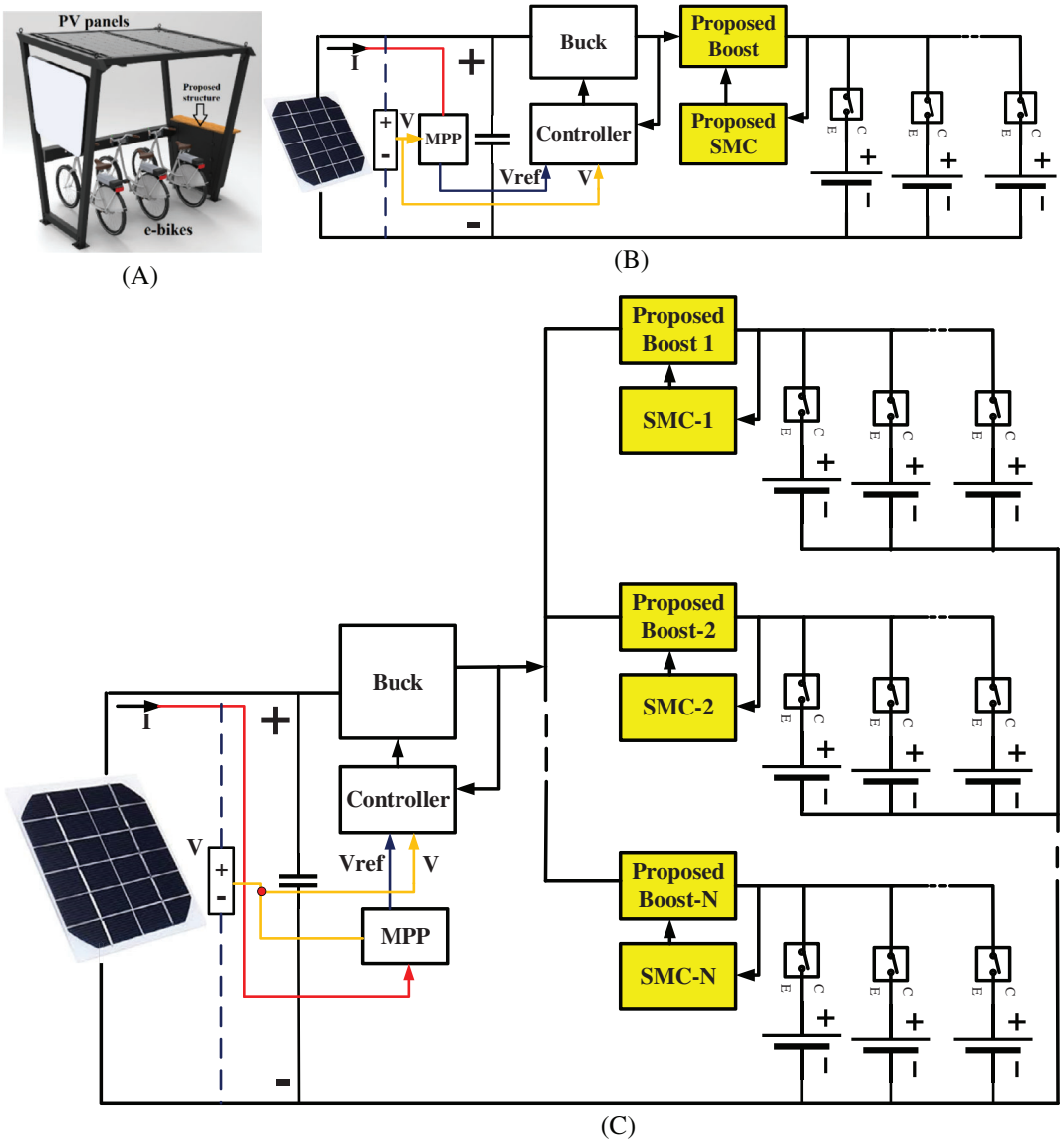

FIGURE 1 A, A simple e-bike battery charging station; B, one-level; and C, multi-level approaches

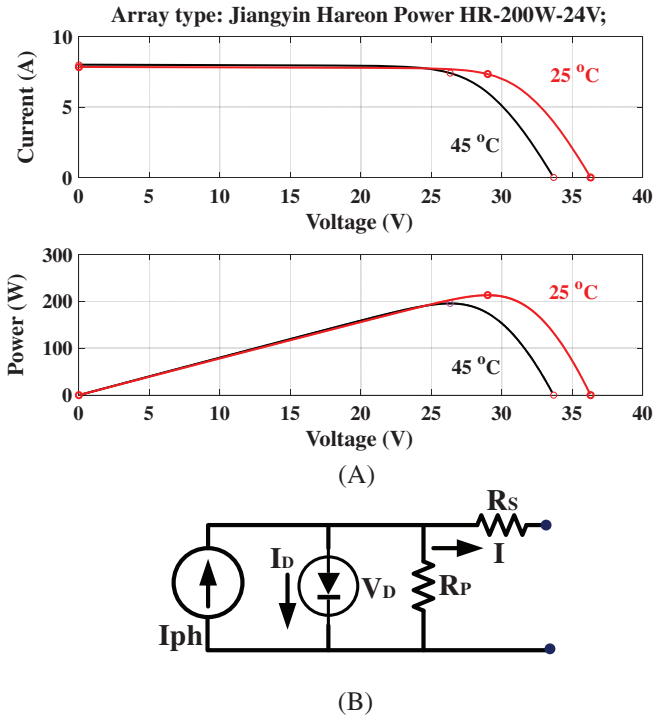

FIGURE 2 A, I-V and P-V characteristics; and B, single-diode solar cell model with series and parallel resistors of the JIYANGYIN HAREON HR-200W-24V PV panel

number of e-bikes that can be connected to the charging station will be determined. This state has been presented in Figure 1B.

Also, we can extend the converter to generate different levels of the voltages to charge all kinds of common utility ranges of voltages for all kinds of the batteries. As can be seen in Figure 1C, different levels of the output voltages can be obtained by multi-level approach of the proposed structure where the boost converters are working separately and the number of the charge stations can be designed based on the power rate of the input PV side.

So, for the simplest condition, for a layer with one battery, this converter is containing a power switch, two power diodes, two capacitors, and an inductor. This figure shows that a combination of PV panels, a current harmonics restrictive filter, a buck converter with a Maximum Power Point Tracking (MPPT) approach, and different boost converters with SMC blocks is applied in this topology. All these parts will be investigated in this part of the study.

2.1 | PV panel

A photovoltaic module (PV module) is made of a combination of photovoltaic cells (PV cells). There are several models for a solar cell, of which the single-diode model is the most common one. Accordingly, a cell can be modeled with a light-dependent current source in parallel with a diode. To make the model more accurate, a series resistor is usually added to the circuit.[28] When the solar cell is exposed to temperature changes (especially at high temperatures), it loses a lot of precision. For this purpose, a parallel resistor is added to the circuit to increase model accuracy at high temperatures. The model with parallel and serial resistors has come to many references.28, 31 Figure 2 shows the photovoltaic cell model.

The electronic components of a photovoltaic system, such as a Buck or Boost converter or a grid-connected inverter, have a minimum and maximum voltage range for input. Therefore, appropriate values for module voltage must be considered to meet specific needs. This partly guarantees the proper performance of the system. But before any voltage calculations, it is important to have an understanding of the output voltage and current of the PV module and how it changes with temperature and sunlight (radiation).

Table 1 and Figure 2A present some electrical and mechanical specifications and I-V and P-V characteristics of the JIYANGYIN HAREON type of PV panel that is used in our application. As can be seen from the figure, the MPP of the panel should be tracked around 200 W and 27.5 VDC.

The current value as a result of light is linearly dependent on the amount of radiation and is expressed as follows:

TABLE 1 Electrical and mechanical specifications of the PV Module HR-200W/24V

Power at MPP (W)	200	Nominal operating cell temp (°C)	45.8
Open circuit voltage temp coefficient (%/°C)	−0.33	Length (mm)	1580.0
Short circuit current temp coefficient (%/°C)	0.05	Width (mm)	808.0
Isc: short circuit current (A)	5.79	Module area (m^2)	1.28

$$I_{ph} = \frac{G}{G_n}\left[I_{ph,n} + k_i(T - T_n)\right] \tag{1}$$

where $I_{ph,n}$ is the nominal current obtained from the radiation in ampere, G and G_n are the amount of irradiation and nominal irradiation respectively in watts per square meter, T and T_n, are the cell temperature at operating conditions and in the nominal state respectively in Kelvin. K_i is the ratio of the short circuit current to the thermal coefficient in terms of amperes per Kelvin.[31]

The diode current is expressed as follows:

$$i_d = I_{sat}\left[\exp\left(\frac{v_d}{\eta V_T}\right) - 1\right] \tag{2}$$

where i_d and v_d are diode current and voltage respectively, I_{sat} is the diode's reverse saturation current and η is the diode's ideal coefficient. The V_T represents the thermal voltage defined as follows:

$$v_T = \frac{k_B T}{q_e} \tag{3}$$

where k_B and q are the Boltzmann constant in term of joules per Kelvin and the electron charge in term of the Coulomb, and T is the cell temperature. By writing KVL and KCL for the circuit of Figure 2B, one can express the solar cell voltage and current equations as follows:

$$I_{ph} - i_d - \frac{v_d}{R_p} - I = 0 \tag{4}$$

$$v = v_d - R_s I \tag{5}$$

The equations stated are for a solar cell. As shown in Figure 1, a module is composed of a series of solar cells. Assuming that the number of cells in the module is N_S, the relation of current and voltage can be written as follows:

$$v_{PV} = N_S v_{cell} \tag{6}$$

$$I_{PV} = I_{cell} \tag{7}$$

The design is considered for around 720 Wh application of charging station. So a parallel connection of four PV panels has been applied in this study.

2.2 | Passive filter

A harmonic problem can be defined as a particular disturbance, which is created by the presence of non-linear components in the electrical system including PV panels as the input sources based on irradiance and temperature values that determine a permanent modification of the voltage and current waves. Passive filters are utilized in electronic systems to protect such systems from harmonic distortion. This protection is usually achieved in a systemic way by creating a reduced impedance path that denies harmonic entrance into the power system.[51] This type of filter consists of passive

components such as resistors, inductors, and capacitors. The simplest way to limit these harmonics is by applying a capacitive filter between the PV panel and the power electronics side. Passive filters are categorized into a low-pass and high-pass filters, that are usually connected in either shunt or series topology. Passive filters are the most utilized type of filters due to their efficiency and significantly low cost.

A low-pass filter can be a single-tuned or doubled-tuned filter. This is a technique of eliminating a particular current harmonic by tuning a low-pass filter to a specific frequency that uses low impedance such as fifth multiples or seventh multiples harmonics of the fundamental. High-pass filters on the other hand also consist of passive components with less impedance for harmonics at specific frequencies thus filtering all harmonic present with higher frequencies.[52] These filters can be configured as the first order, second order, third order, and fourth-order high-pass filters. The first order filters are the simplest form of high-pass filters, containing only one passive component. The order of the high-pass determines the number of component(s) contained in the filter and the higher-order provides better stability to the power system. In our study since we are focusing on the SMC based multi-level boost converters, we simply applied a capacitor between the PV panel and buck converter. Also, the MPPT algorithm of the buck converter helps to decrease the current harmonics of the topology and increase the efficiency.

2.3 | Buck converter

In different working conditions of solar cells (sunrise, noon, sunset), the panels have a certain instantaneous power, which is the voltage of the panels multiplying the current of the panels.[28] Now, if we divide the voltage over the current, the internal resistance of the panels at that moment will be obtained for a certain amount of sunlight. According to the basic power calculation rules, the maximum load power must be equal to the resistance of the other parts of the circuit (RL = Rth). Because the sun is moving throughout the day, the intensity of the radiation varies and the amount of current and voltage of the panels will also vary.

Here the MPPT system comes into play, keeping the panels' internal resistance equal to the load resistance, allowing maximum power to be transmitted throughout the day. MPPT performs the impedance matching by varying the voltage and current of the panels. Obviously, if the load resistance changes, then the current and voltage values of the panels will be changed by MPPT. As shown in Figure 1, as the intensity of sunlight increases, at a constant voltage, the current rate of the cells increases. A consumer with $R = V/I$ resistance should be able to receive "maximum power" from the panels, or in other words, have the power to be equal to the maximum power point of the panels at that moment (curved knee in Figure 2), in which case the internal resistance of the panels should be equal to the load resistance. The internal resistance of the panels is a variable parameter and depends on factors such as the amount of irradiance and the temperature of the panels. If this resistance is more or less than the load resistance, the load transfer power will not be maximal, in other words, the gain of the panels will decrease. MPP detectors employ a variety of methods to find the maximum power and maintain the efficiency of the solar cells at maximum value.

In our study the Perturbation and Observation (P&O) algorithm has been applied. In this method, the controller changes the panel voltage slightly, and if the output power is increased compared to the previous state, the voltage will continue in the same direction until the output power remains constant. This is the most common method and the algorithm has been illustrated in Figure 3. The amount of ΔV is adjusted to 0.05 V and sampling frequency is 50 KHz.

2.4 | Boost converter

The conventional and selected boost converters have been presented in Figure 4A,B respectively. As can be seen, the number of components is the same for both configurations. Both these converters have investigated in different researches and mathematical analysis of the selected converter is reported in References 53 and 54. Our study presents a comprehensive analysis of this converter and the performance of this structure is investigated under three different PID, FLC, and proposed SM-based controllers. But if we want to compare the advantages and disadvantages of the converters, we should say that changing the location of the inductor in the circuit can give us limited dynamic losses because of the smaller current values in the inductor and it can improve the efficiency of the converter.

On the other hand, the voltage and current stresses of the power switch are smaller for the proposed converter, based on the serial connection of the inductor that can act as a snubber inductor, and also the first capacitors C_1 can

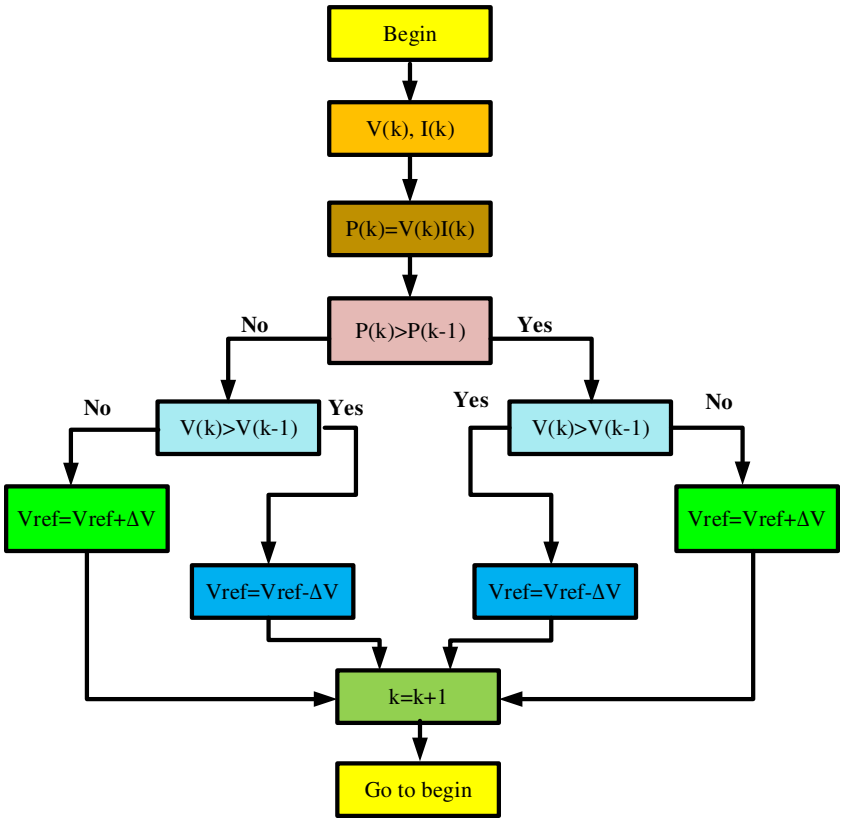

FIGURE 3 P&O algorithm for MPPT of PV panel through Buck converter

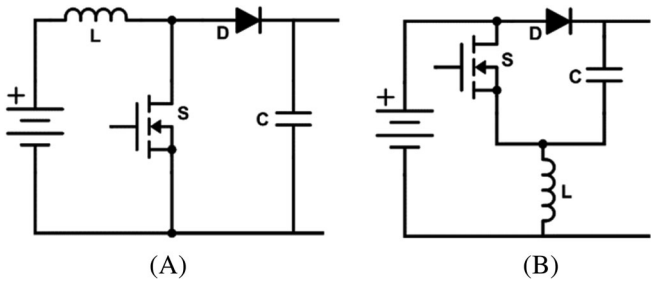

FIGURE 4 A, Conventional and (B) proposed boost converters

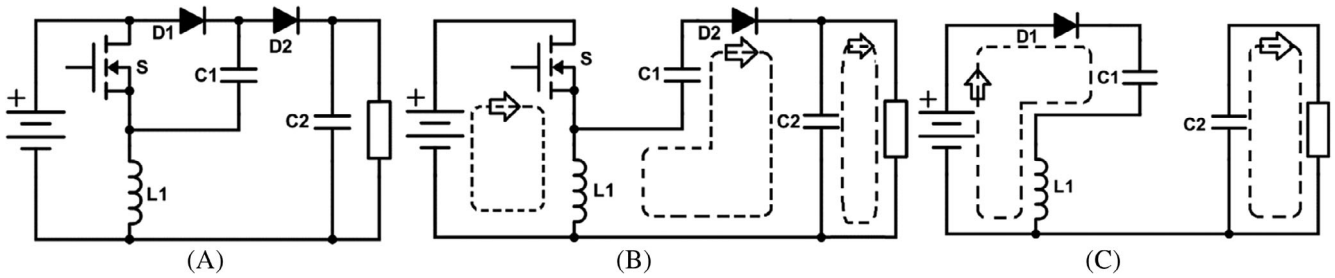

FIGURE 5 A, The proposed converter with one level of the output voltage and its state when the power switch is in (B) on and (C) off states

role as a snubber capacitor. So the current and voltage changes will be softer and the reliability and long-life will increase.

Figure 5A illustrates this state. Figure 5B,C shows the state of the converter when the power switch is in ON and OFF modes respectively.

Since the most important factor is current for a charge station, so working in Discontinuous Current Mode (DCM) can lead to unstable charging conditions. For this project, the desired state of all converters in all blocks is working ability in Continuous Current Mode (CCM). So, the performance of the converter should be considered in this state. This operation state is including two different ON and OFF modes of the power switch. The state of all components can be followed through Figure 6.

Mode 1: When the gate-source pins of the power switch receive the pulse and switch goes to ON mode, the inductor L_1 begins to charge through the switch by the input voltage source. In this state, the voltage of the anode pine of the diode D_1 will be smaller than the cathode's voltage and so it will be in reverse bias station and turns off. The voltage on the capacitor C_1 will be discharged on the load through the diode D_2 and the output capacitor begins to charge. All of these states can be followed through Figures 4 and 6. For this state, based on described facts we can write:

$$V_{\text{in}} = V_{\text{L}} \tag{8}$$

$$V_{\text{L}} = V_{\text{O}} - V_{\text{C1}} \tag{9}$$

$$V_{\text{C2}} = V_{\text{O}} \tag{10}$$

V_{in} and V_{O} are the input and output voltages of the boost converter, V_{C1} and V_{C2} are the voltages on capacitors C_1 and C_2 respectively.

The current equation for the input side of the converter when the switch is in on mode can be presented by:

$$i_{\text{in}} = i_{\text{L}} + i_{\text{C1}} \tag{11}$$

And for the output side we can obtain:

$$i_{\text{CO}} = i_{\text{C1}} - I_{\text{O}} \tag{12}$$

Also as can be seen from Figure 4B, the current of the diode D_2 is equal with:

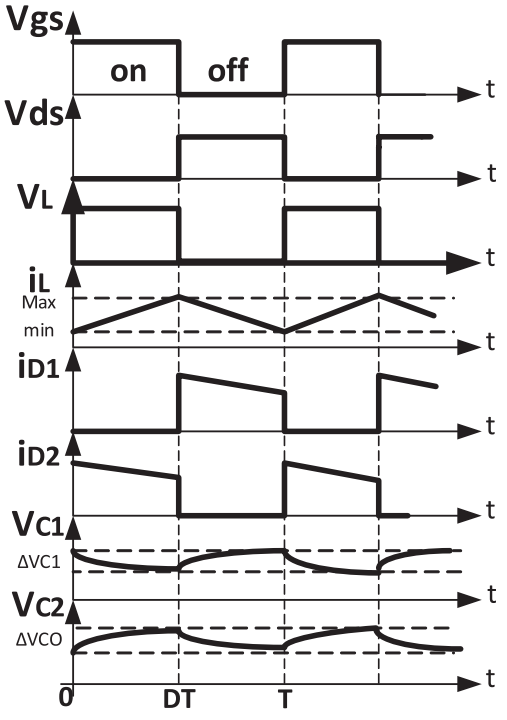

FIGURE 6 The state of all the components in proposed converter

$$i_{D2} = i_{C1} \tag{13}$$

Mode 2: In this mode, the power switch will be turned off and the diode D_2 is reversed biased. Through this state, the current on the L_1 will charge the capacitor C_1 and the voltage on capacitor C_2 will discharge on the load. So, for this state we can have:

$$V_L = V_{in} - V_{C1} \tag{14}$$

$$V_{C2} = V_O \tag{15}$$

The current equations for the input and output sides of the converter in off mode can be illustrated by:

$$i_{in} = i_L = i_{C1} = i_{D1} \tag{16}$$

$$i_{CO} = -I_O \tag{17}$$

For a boot converter, duty cycle can be presented by:

$$D = \frac{T_{on}}{T} = \frac{T_{on}}{T_{on} + T_{off}} \tag{18}$$

T_{on} and T_{off} are the time intervals that the switch is in ON and OFF stats respectively.
For the steady-state conditions, by considering the voltage balance principle on the inductor L, we can obtain:

$$\int_0^{DT} V_{L,on} dt + \int_{DT}^{T} V_{L,of} f dt = 0 \tag{19}$$

Also, for this condition we can write for the capacitor C_1:

$$V_{C1} = \frac{V_{in}}{1-D} \tag{20}$$

By replacing Equations (9), (17), (20), we can obtain:

$$M = \frac{2-D}{1-D} \tag{21}$$

M is the gain of the proposed converter for the CCM state. For the current equations, based on the same principle in steady-state conditions:

$$\frac{1}{Ts}\left(\int_0^{DT} i_{C2,on} dt + \int_{DT}^{T} i_{C2,of} f dt\right) = 0 \tag{22}$$

That can be obtained:

$$i_{C1,on} = \frac{I_O}{D} \tag{23}$$

So for the capacitor C_1 by using Equations (11), (16), (22) we can calculate:

$$i_{C1,off} = -\left(\frac{I_O}{1-D}\right) \tag{24}$$

So, the oscillation of the capacitor voltage can be found through (25):

$$\Delta i_{C1} = \frac{I_O}{D(1-D)} \tag{25}$$

This principle will result for the input and output current:

$$\frac{1}{Ts}\left(\int_0^{DT} i_{C1,off}dt + \int_{DT}^{T} i_{C1,off}dt\right) = 0 \tag{26}$$

And,

$$i_{C1,off} = \frac{I_O}{1-D} \tag{27}$$

If we consider all the components ideal, by applying (21), we can write:

$$\frac{I_O}{I_{in}} = \frac{2-D}{1-D} \tag{28}$$

That can give us the current relation for the converter by considering the input and output currents. By considering both the on and off states for the converter:

$$I_{in} = \frac{i_{in,on} + i_{in,off}}{2} = \frac{2-D}{1-D} I_O \tag{29}$$

By replacing Equation (27) into (29):

$$i_{in,on} = \frac{3-2D}{1-D} I_O \tag{30}$$

By applying Equations (12), (17), (22), we can obtain:

$$i_{C2,on} = \frac{1-D}{D} I_O \tag{31}$$

And the current ripple on the output capacitor can be calculated by:

$$\Delta i_{C2} = \frac{I_O}{D} \tag{32}$$

In comparison with the conventional step-up converter, based on Equation (21), it is evident that the proposed converter by considering the same number of the components has a higher DC voltage gain. Table 2 presents different structures to evaluate the voltage gain and stresses on the power switch. But we should consider that for an e-bike charging station, the main important issue is the converter's ability in the current generation for the batteries and the number of the components and power elements. For this purpose, the voltage gain of the converter is not very important.

TABLE 2 Comparison between converter's voltage gain and stresses

Converters	Proposed with 1 block	Proposed in cascaded 2 block	37	38	39	55 with n = 2
Number of switches	1	2	2	2	2	3
Number of inductors	1	2	8	2	3	2
Number of diodes	2	3	4	3	2	4
Number of capacitors	2	3	4	3	3	3
Total components	6	10	18	10	10	12
DC voltage gain	(2 - D)/(1 - D)	((2 - D)/(1 - D)2) + 1	(2[1 + D])/(1 - D)	(3 - D)/(1 - D)	(1 + 3D)/(1 - D)	1 + nD/(1 - D)
Voltage stress on switch	Vo/(2 - D)	Vo/(3 - 3D + D2)	Vo/(2[1 + D])	Vo/(3 - D)	Vo/(1 + 3D)	Vo/(1 + nD)
Total voltage stresses	Vo/(2 - D)	Vo/(3 - 3D + D2)	Vo/(2[1 + D])	Vo/(3 - D)	Vo/(1 + 3D)	Vo/(1 + nD)

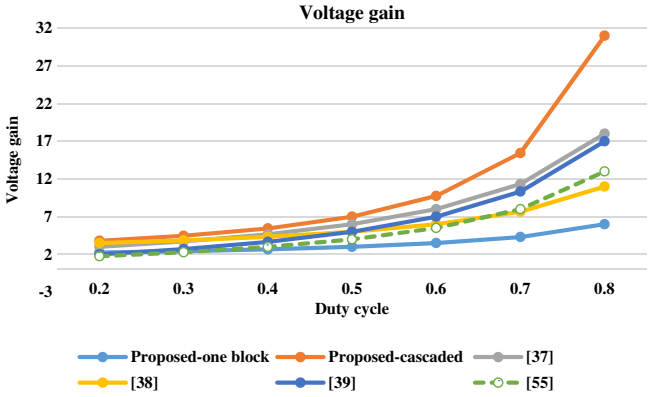

FIGURE 7 The voltage gains comparison curve for different converters

Although for our design, high voltage stresses will not occur based on battery charging voltage level, but this converter can also be used for high gain applications for other purposes especially with cascade topologies. So, in this table, for one and two cascaded blocks, the voltage stresses, voltage gain and number of the components have been written.

For a two blocked-cascaded topology of the proposed converter, the number of the components is the same as topologies proposed in References 38 and 39. Reference 37 contains three pairs of coupled-inductors and two independent inductors and[39] presents a topology with three inductors. So the total values of the losses can be high for these structures and the control process of the converter is difficult for these power switches. Topology in Reference 55 is containing three power switches that result in a complex control model and more components. Figures 5 and 6 show a comparison for the voltage gain and stresses on the switches of the structures presented in Table 2. The voltage stresses for the cascaded topology of the proposed converter is considerable especially for the duty cycles equal and greater than 0.5. Since we will apply the one-phase approach of the proposed converter and do not need to enhance the voltage on the battery side, the voltage stresses are not a serious problem in our structure in a single block state. But if we consider the structure for other purposes for high gain converters, the voltage stresses and dc gain of the cascaded structure are in a very good category based on results presented in Figures 7 and 8.

Figure 9 presents the efficiency diagram for the mentioned converters in Figures 7 and 8. As can be seen, the efficiency of the selected converter in one-block structure is acceptable for low and high power applications and has the best response in a general comparison for all powers, where this converter under control process of the proposed SCM controller is tested for 700 till 800 W applications. It is important to mention again that all component values for the selected converter are less than all other investigated converters where especially the number of power switches and inductors are less and lower losses are predictable.

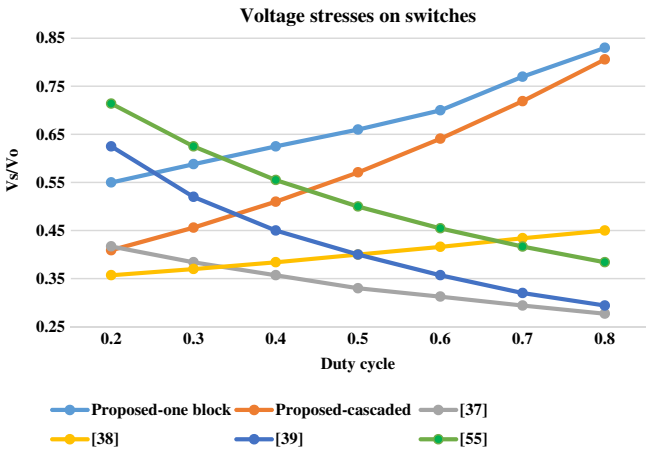

FIGURE 8 The voltage stress of the power switches comparison curve for different converters

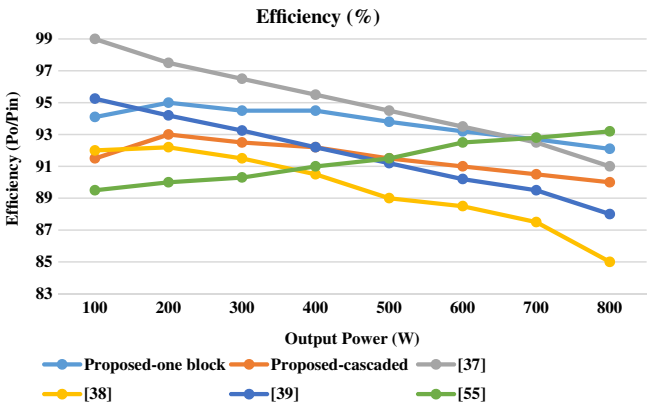

FIGURE 9 Efficiency comparison curve for different converters

3 | THE THEORY OF THE PROPOSED SMC

The steady-space matrices for a circuit can be suggested by writing the n-first derivative equations for the current of the independent inductors and voltages of the capacitors. The general equation of this state can be presented by:

$$\dot{x} = Ax + Bu \tag{33}$$

u and x in (33) are the input sources and the first-order current derivatives of the inductors and voltage derivatives of the capacitors respectively. This term is well-known as the state vector. A and B are the state coefficients matrices. As discussed in section 2, the CCM working condition should be considered for this study. So, in the first step, we should model the converter for both ON and OFF states of the converter. For the time interval that power switch is in ON mode, $u = 1$, based on Figure 3B:

$$L\frac{di_L}{dt} = V_{\text{in}} \Rightarrow \frac{di_L}{dt} = \frac{V_{\text{in}}}{L} \tag{34}$$

$$V_{\text{C1}} = V_{\text{in}} - V_{\text{C2}} \Rightarrow \text{C}_1\frac{dV_{\text{C1}}}{dt} = -\text{C}_2\frac{dV_{\text{C2}}}{dt} \tag{35}$$

$$\text{C}_1\frac{dV_{\text{C1}}}{dt} = \text{C}_2\frac{dV_{\text{O}}}{dt} + \frac{V_{\text{O}}}{R} \tag{36}$$

Since $V_{\text{CO}} = V_{\text{C2}}$, by replacing Equation (35) into (36), we can write:

$$-\mathrm{C}_2\frac{dV_{\mathrm{C2}}}{dt}=\mathrm{C}_2\frac{dV_{\mathrm{O}}}{dt}+\frac{V_{\mathrm{O}}}{R}\Rightarrow\frac{dV_{\mathrm{C2}}}{dt}=-\frac{V_{\mathrm{O}}}{2\mathrm{C}_2R} \tag{37}$$

And Equation (35) can be re-written by:

$$\mathrm{C}_1\frac{dV_{\mathrm{C1}}}{dt}=\frac{V_{\mathrm{O}}}{2\mathrm{C}_2R} \tag{38}$$

For the OFF state of the power switch, we can write the steady space vectors as below through Figure 3C:

$$(V_{\mathrm{in}}-V_{\mathrm{C1}})(1-d)=L\frac{di_L}{dt}\Rightarrow\frac{di_L}{dt}=\frac{(1-d)}{L}V_{\mathrm{in}}-\frac{(1-d)}{L}V_{\mathrm{C1}} \tag{39}$$

$$i_L(1-d)=\mathrm{C}_1\frac{dv_{\mathrm{C1}}}{dt}\Rightarrow\frac{dv_{\mathrm{C1}}}{dt}=\frac{1-d}{\mathrm{C}_1}i_L \tag{40}$$

$$\mathrm{C}_2\frac{dv_{\mathrm{CO}}}{dt}=\frac{V_{\mathrm{O}}}{R}(1-d)\Rightarrow\frac{dv_{\mathrm{CO}}}{dt}=\frac{V_{\mathrm{O}}(1-d)}{\mathrm{C}_2R} \tag{41}$$

(1-d) will guarantee that the converter is working in the OFF state. So, by considering the Equations (34) till (41), we can re-organize the steady-space total matrix as Equation (42):

$$\begin{aligned}\frac{di_{L1}}{dt}&=\frac{(2-d)}{L_1}V_{\mathrm{in}}-\frac{(1-d)}{L_1}V_{\mathrm{C1}}\\ \frac{dv_{\mathrm{C1}}}{dt}&=\frac{(1-d)}{\mathrm{C}_1}i_{L1}-\frac{1}{2\mathrm{C}_2R}V_{\mathrm{O}}\\ \frac{dv_{\mathrm{o}}}{dt}&=\frac{V_{\mathrm{O}}(1-2d)}{2\mathrm{C}_2R}\end{aligned} \tag{42}$$

$$\begin{bmatrix}\dot{i}_{l1}\\ \dot{v}_{c1}\\ \dot{v}_o\end{bmatrix}=\begin{bmatrix}0 & -\frac{1-d}{L_1} & 0\\ -\frac{1-d}{\mathrm{C}_1} & 0 & \frac{1}{2\mathrm{C}_2R}\\ 0 & 0 & \frac{1-2d}{2\mathrm{C}_2R}\end{bmatrix}\begin{bmatrix}i_{L1}\\ v_{\mathrm{C1}}\\ v_{\mathrm{CO}}\end{bmatrix}+\begin{bmatrix}\frac{2-d}{L_1}\\ 0\\ 0\end{bmatrix}[V_{\mathrm{in}}] \tag{43}$$

Components values in order to work in the CCM is one of the most important issues and should be chosen properly. For a DC-DC boost converter, the critical inductor and capacitor values defined by Equation (44):

$$L_{\mathrm{C}}=\frac{Rd}{2f_{\mathrm{S}}}(1-d)^2 \tag{44}$$

$$C_{\mathrm{C}}=\frac{V_{\mathrm{oe}}d}{Rf_{\mathrm{S}}\Delta V_{\mathrm{oe}}} \tag{45}$$

In these equations, d, R, f_{S}, V_{o} and ΔV_{oe} are the duty cycle, output resistive load, switching frequency of the power switch, output voltage, and the ripple value of the output voltage respectively. So, by selecting an inductance above the L_{C} and a capacitor through Equation (45) by considering an appropriate ripple value for the output voltage, the CCM condition will be guaranteed.

The main goal of applying a DC-DC boost converter is fixing the output voltage at the output side of this converter even by changing the output load or input voltage conditions. Based on the SMC theory, in the state-space, the time-variant Sliding Function (SF) is determined by Equation (46):

$$S_S = K_1(t) \times (V_{oe} - V_o) \tag{46}$$

In this equation, $K_1(t)$ is the Sliding Coefficient (SC) and can be chosen time-variant or fixed based on availability, reach/strike and stability condition. Since $K_1(t)$ is the fixed part during different steady-states in this control model, its derivative will be equal with zero. So, the differential FC is presented by Equation (47):

$$\dot{S}_S = -K_1(t)\dot{V}_o \tag{47}$$

Resulting in equivalent control given by Equation (48):

$$V_{eq} = 1 - \frac{V_o}{Ri_L} \tag{48}$$

In Equation (48), the V_{eq} is the equivalent control signal. By considering the last equation, the coincident trending law S_L, can be identified by Equation (49):

$$S_L = -K_2(t)(V_{oe} - V_o) \tag{49}$$

By adjusting the coefficient $K_2(t) > 0$, the trending speed can be regulated and fixed. The sliding function conditions should be considered general in order to regulate the output voltage of the DC-DC boost converter by tracking of the reference voltage. These conditions are illustrated by:

$$V = \begin{cases} V^+, & \text{if } S_S \rangle 0 \\ V^-, & \text{if } S_S \langle 0 \end{cases} \tag{50}$$

The dynamic duty cycle of the pulse width modulation signal for the power switch in order to fix the output voltage in the desired value can be found by:

$$0 \langle d(t) = 1 - \frac{K_1 V_i + \sqrt{K_1{}^2 V_i{}^2 + K V_o (V_{oe} - V_o)}}{2K_1 V_o} \langle 1 \tag{51}$$

In this equation, V_i is the input voltage, and K is defined by:

$$K = \frac{4L\left(CRK_2{}^2 - K_1 K_2\right)}{R} \tag{52}$$

In order to prove the correctness of Equation (52), when the difference between real and reference voltages at the output side of the boost converter is zero, $d(t)$ will be equal with:

$$d(t) = 1 - \frac{V_i}{V_{oe}} \tag{53}$$

The main specification of Equations (51)–(53) is the controller independence from the inductor current and as can be seen, the control process can be done through the values of the physical components such as inductor, capacitor and resistive load values and input, desired output and sliding coefficients. Since the values of the components are certain, so the control process will be done through these coefficients. Figure 10 presents the proposed configuration and

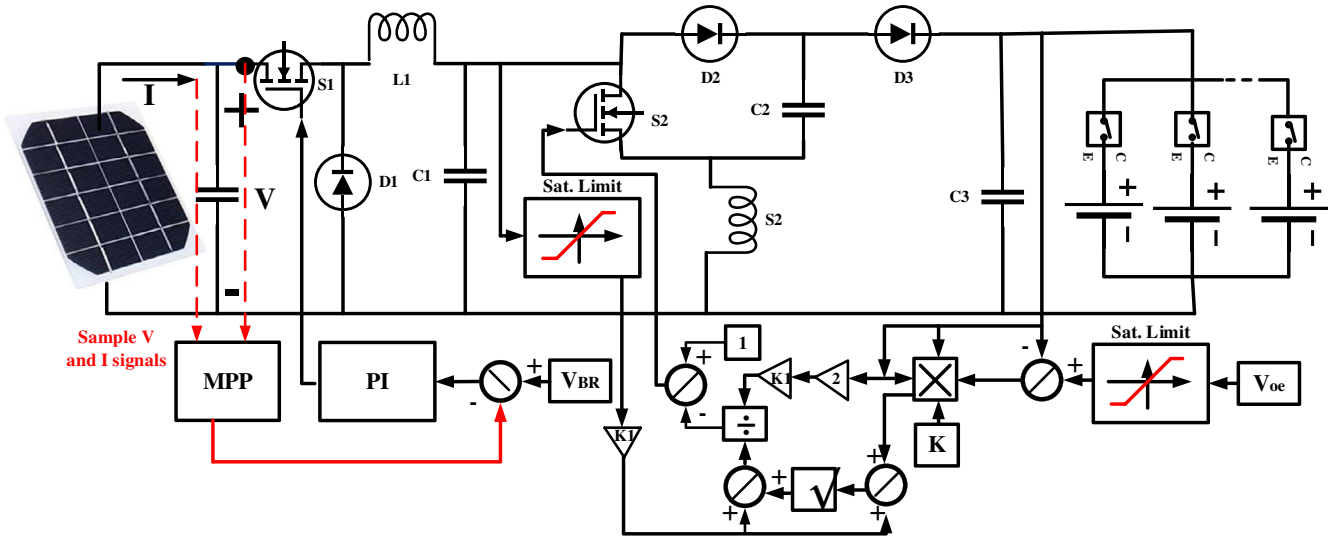

FIGURE 10 Proposed PV-based e-bike charging station

Input voltage (VDC)	L(μH)	R_L (Ω)	C (μF)	R_{OUT} (Ω)	f_S (KHz)
18	220	0.022	220	3.6	50

TABLE 3 Components values for the all controllers in boost converter side

controller topology. For the buck converter side, a conventional step-down converter with a PI controller has been considered and we focused on the boost converter side and the proposed SMC. For the buck side, one power switch, one diode, one inductor, and one capacitor are applied. The output voltage of this block will compare with the VBR = 18 VDC as the reference voltage level for the block and controller is regulating the output of this converter at the 18 VDC. The second block is containing one power MOSFET, one inductor, two diodes, and two capacitors. The output voltage of this block is comparing with the VOE = 36 VDC as the reference voltage and the coefficient K is determining from Equation (53). Control laws specified in Equations (50)–(52) and initial starting points in the state-space model, optional external points (negative or positive area) or on the sliding surface S_S, within a finite time will reach to the S_S. This means that the designed control law meets the reaching condition. We can prove this issue in this way: if $S_S < 0$, the obtained voltage value will be more than the requested voltage and based on the controller performance, the duty cycle will decrease to regulate the voltage to the desired value. As a result, the voltage will reach the sliding surface. If $S_S = 0$, the desired and obtained voltages are the same and so the controller keeps the duty cycle at the critical value without any change. For the final possible state, if the $S_S > 0$, it shows the obtained voltage at the output ends of the converter is below the reference voltage and the controller gives longer duty cycles to the switch in order to reach the desired voltage.

4 | SIMULATION AND EXPERIMENTAL RESULTS

This section is presented in order to analyze the performance of the MPPT algorithm for increasing the input current quality in buck converter and the proposed SMC for the boost converter. A broad simulation group has been done and results for SMC have been compared with PID and fuzzy-based controllers and reported in this section. The MATLAB/SIMULINK has been selected for the simulation assessment. All components values are considered the same for all controllers as shown in Table 3.

As previously described a buck converter is located between input PV panels and the boost converter to fix the input voltage of the boost converter. As reported in section 2, the purpose of applying this converter is enhancing the current values since the most important parameter is current in the e-bike charging stations. On the other hand, because of the different voltage values for different batteries from 36 VDC till 54.5 VDC, and by considering the output voltage of the panels that can reach sometimes to more than 36 VDC according to the geographical and weather conditions, it is

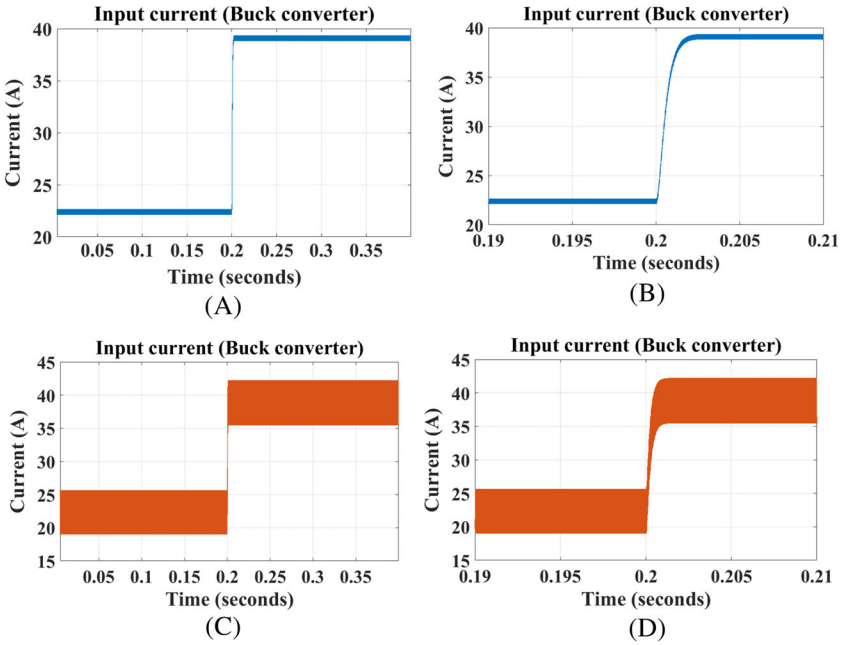

FIGURE 11 The quality of the current signal for buck converter, (A), (B) after and (C), (D) before placement the filter

needed to decrease the panels voltage to a lower grade and amplify the current by this block. Based on different working conditions for the PV panels and variable irradiance and temperature parameters, the current of these panels may contain a high THD value and large ripple. As described in section 2.2, a simple capacitive filter with 2 mF capacity is located between the PV panel and buck converter to decrease these undesirable factors. A simulation has been done to show the quality of current signals before and after the placement of the filter. The results are shown in Figure 11. Figure 11A presents the filter's input current and Figure 11B illustrates the ripple of this current magnitude in a focused situation around the $t = 0.2$ that the second e-bike connects at the load side. Figure 11C,D presents the quality of the input current without considering the filter. A large-amplitude for the ripples can be observed through this figure.

For the boost block, the amount of the inductor and capacitor have been selected based on Equations (44) and (45) in order to guarantee the working condition in the CCM state. Also, in order to present the actual conditions in the inductor, a resistance with a serial connection has been added to the inductor. For the experimental prototype, we applied a 220 μH inductor, we measured the resistance of the inductor and applied the same value for the simulation results. Where we suggest a 10 Ah converter, so a 3.6 Ω resistor is added to the converter's output ends. For the second stage, the same value of the resistor will add by a parallel connection with the first load to play the role of the second bicycle as presented in Figure 1B. Figure 12 presents the results of the simulations. For all proposed SMC, FLC, and PID controller based converter, both output voltage and input and output currents waveforms are reported in this figure. Figure 12A,B illustrates the output voltage of the converter and input and output currents of the converter under the PID controller. Based on supposition, at the $t = 0.1$ second, the second e-bike will be connected. As can be seen and predicted from Figure 12A, the tracking process of the desired voltage is slow in this controller and especially after adding the second load, it needs more time to receive to the 36 VDC again. About the current, the same rate of the tracking problem seems and before reaching the final values for the voltage and current the second load is applied.

For the Fuzzy Logic-based controller, the track of the desired voltage is quicker rather than the PID controller, but the ripple values for the voltage and current still are appearing. These all can be seen from Figure 12C,D respectively. The proposed sliding mode controller results are shown in Figure 12E,F for the voltage and currents respectively and quickest responses are reported by this method. Where the PID and FLC need to 0.1 and 0.035 seconds to reach the final voltage value, this controller regulates the output voltage is less than 0.01 second as can be seen from Figure 8E and the final value of the current 20 A, for two bicycles, with less ripple and near to this value is reported for the projected controller.

As previously described, the need for a multi-level approach is due to the existence of different battery types in the market with various levels of charging voltages. So, the proposed topology should be able to generate different levels of the voltages and be robust against more e-bike connections as the loads in the charging station.

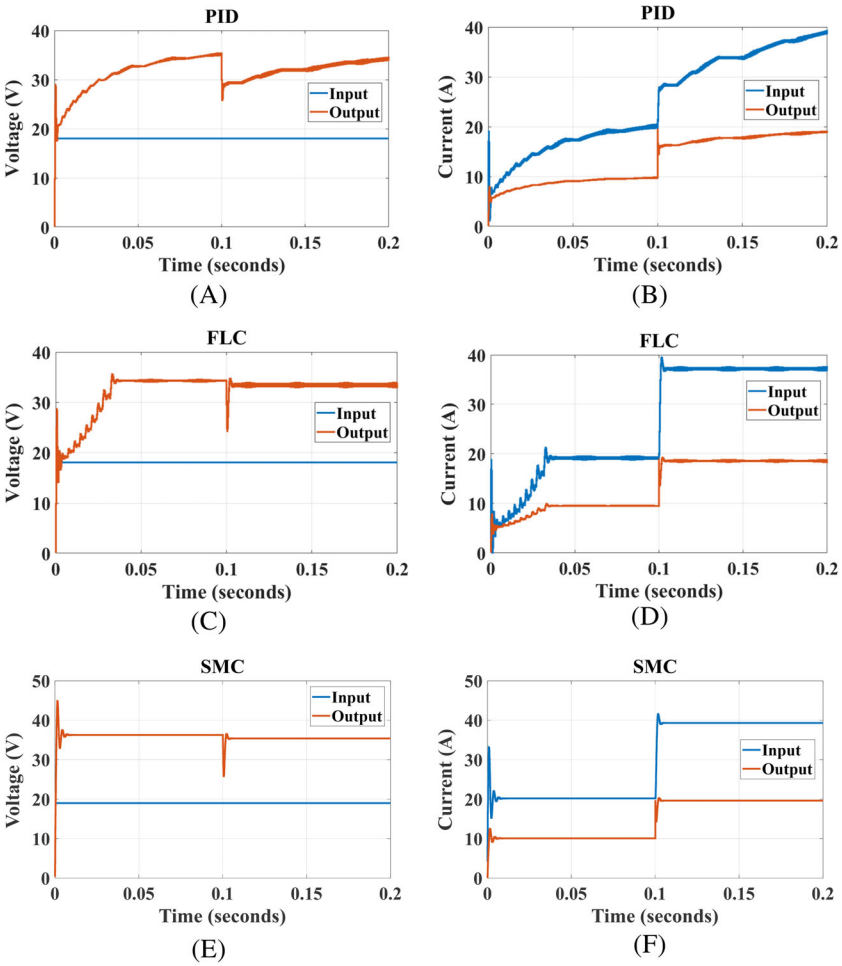

FIGURE 12 Performance assessment of the PID, FLC and proposed SMC for e-bike station with two loads, when V_{OUT} = 36 VDC

Based on Figure 1C, Figures 12 and 13 present a multi-level approach of the selected converter under PID, FLC, and SMC-based controllers. This simulation has been done in order to analyze the performance of controllers for obtaining a fixed 36 VDC and 42 VDC at the output ends of the boost converter by applying more than one battery. Figure 13 illustrates the results of the 42VDC approach. Figure 13A presents the input and output voltages for the converter with PID controller and comparatively a slow track is reported. The most negative aspect of this figure is the controller performance when the second battery is connected at the $t = 0.1$ second and has suffered a large voltage drop. Figure 13B presents the input and output currents for this controller. Although a large transient time has been reported, but the currents are in a proper situation.

Figure 13C,D preset the input and output voltage and current waveforms for the projected converter under FL controller. The reverse behavior of this controller is remarkable, where the second load is connected. An undershoot and then an overshoot is reported. This behavior can be explained when the total load value is expected to decrease when two loads are connected in parallel. Although, this condition is same for all controllers, but the behavior of FLC is an unexpected situation. The currents are in a good level and in comparison with PID, a higher level of current in FLC is reported. As can be seen from Figure 13E,F, the best responses are given by proposed SMC technique. A very limited value of voltage drop around 1VDC is obtained for output voltage and the current value drawn from the source is less for this controller.

Figure 14 illustrates the PWM pulses generated by these methods and as can be seen, per controller works in a different algorithm and generates different waves. Because of the frequency of the PWM signals the first 0.0035 second and final 0.005 second of the time have been reported. Figure 14A,D presents the result of the PID controller, Figure 14B,E illustrates the results of the FLC method and Figure 14C,F is reporting the results of the SMC. Among all the results, PID and SMC act similarly because of the mathematical basis of these controllers. FLC works according to the trial and error, so the generated PWM is more intensive.

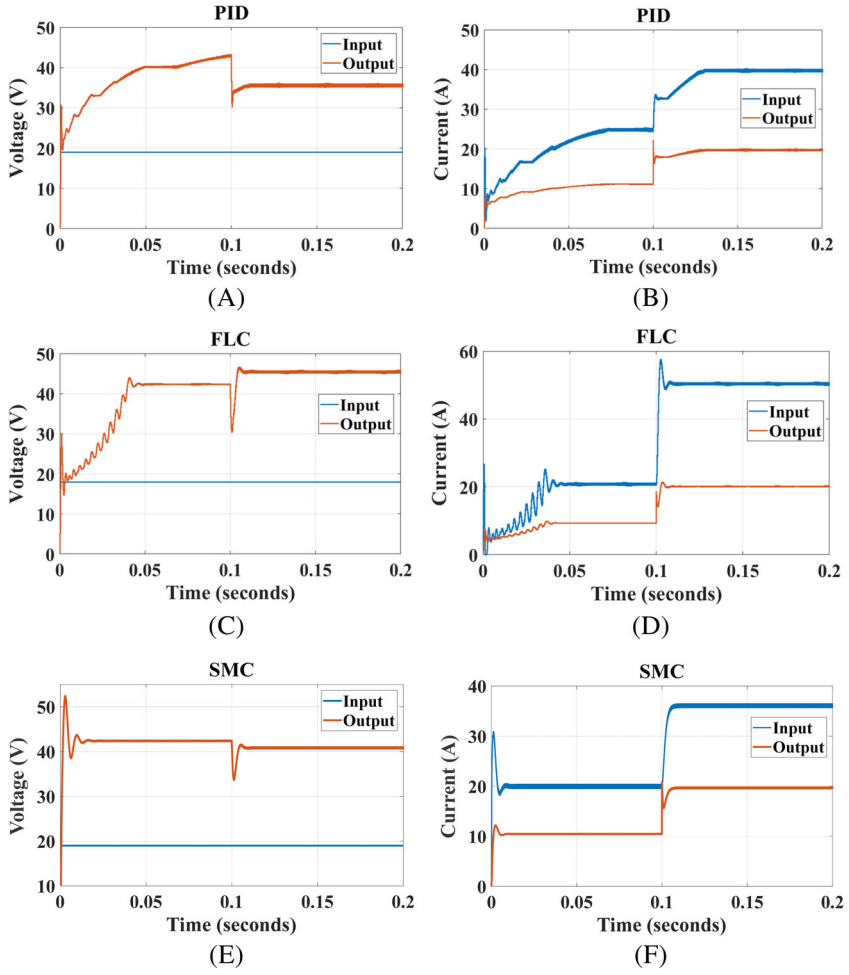

FIGURE 13 Performance assessment of the PID, FLC, and proposed SMC for e-bike station with two loads, when $V_{OUT} = 42$VDC

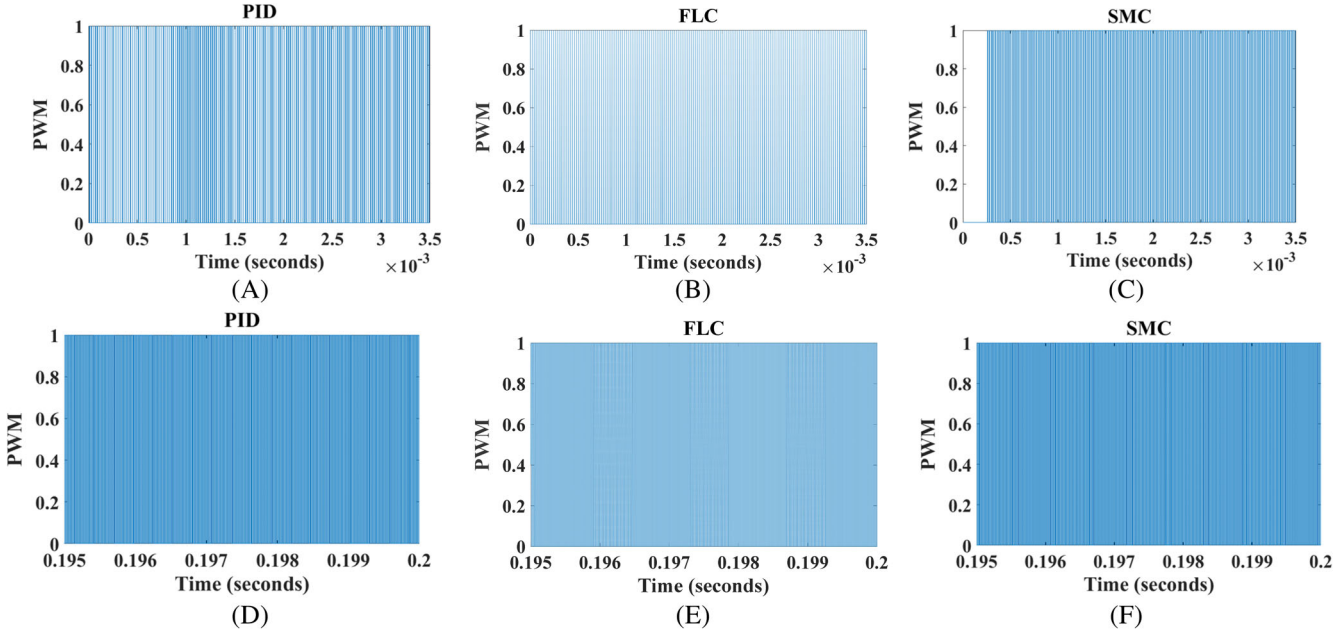

FIGURE 14 Generated PWM signals for the power switch by different controllers

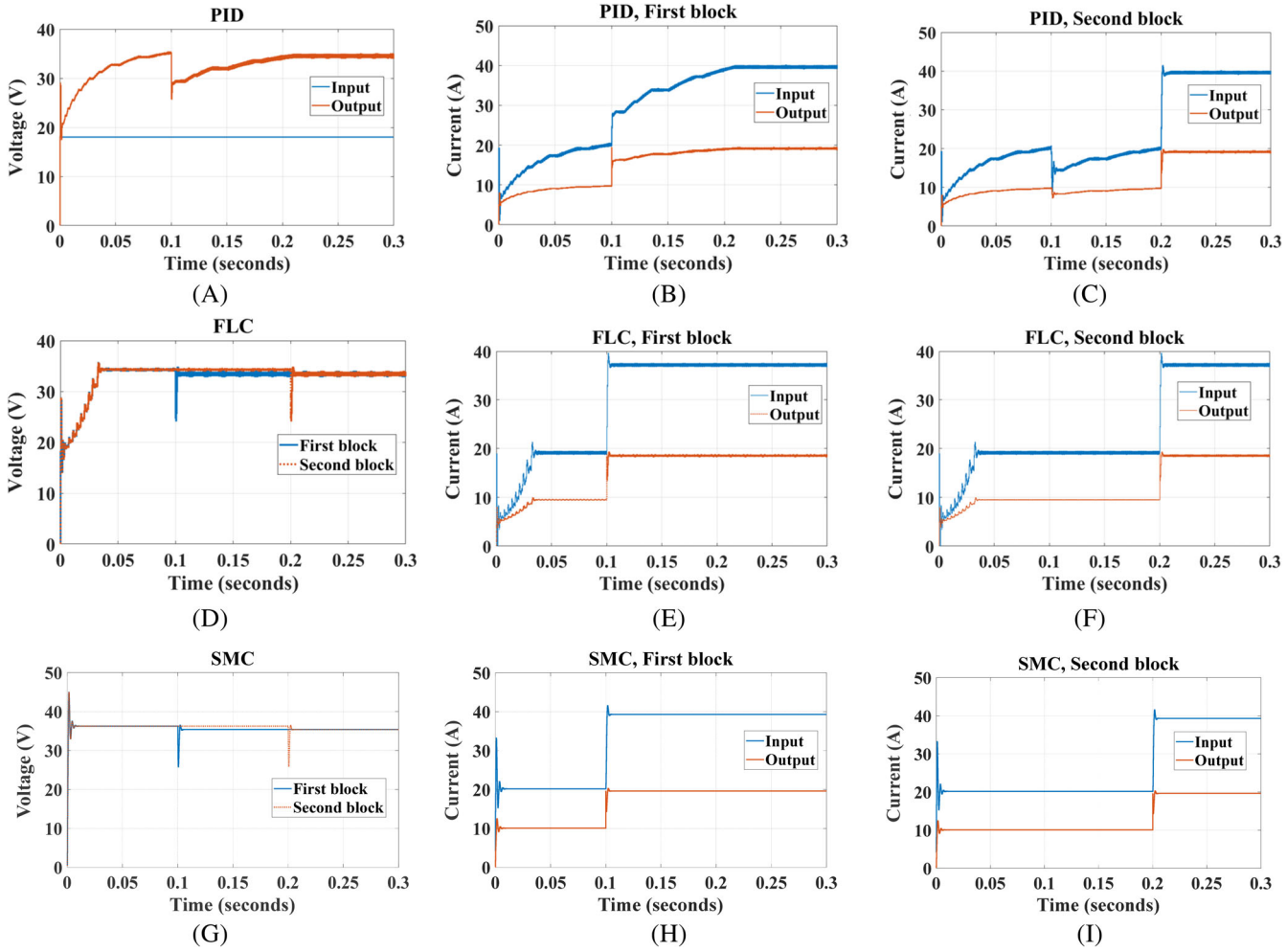

FIGURE 15 Performance assessment of the PID, FLC and proposed SMC for e-bike station with two blocks and two loads for per block

Figure 15 presents the result of the simulations for the designing presented in Figure 1C for a fixed 36 VDC for both blocks. For this purpose, we considered two different blocks and two loads for per block. Per block containing a boost converter and different PID, FLC, and SMC controllers and any of the blocks are feeding two e-bikes. For the first block, the second load will inter in the output ends of the converter at the $t = 0.1$ second and for the second block, the second load will add at the $t = 0.2$ second. The same results are obtained for this configuration.

In comparison with the results presented in Figure 12, the SMC presents quicker response and acceptable droops of the voltage at the load's connection moments, $t = 0.1$ and 0.2 seconds in this simulation. PID controller still is slow and FLC is quicker in comparison with PID and slower rather than SMC and has more overshoots at the connection points of the other loads. Figure 15A,D,G presents voltage waveforms of the proposed converter and controllers for a two-block topology. Figure 15B,E,H illustrates the performance of the controllers when a new load is connected for the first block and Figure 15C,F,I shows the same results for the second block. As mentioned, the second e-bike for the first and second blocks of boost converters is connected at the $t = 0.1$ and 0.2 seconds respectively.

Figure 16 presents the generated pulses for the power switch of per block for different controllers and it simply confirms the result given in Figure 14. As can be seen, the most intense pulses are generated by FLC that uses of control rules and SMC and PID controllers generate more regular pulses.

Figure 16A,D presents the result of switching signals under the PID controller, Figure 16B,E illustrates the driving signals for the FLC and Figure 16C,F shows the same signals under the proposed SMC. Figure 17A,B shows the comparison between input and output currents for the proposed and conventional converters. As discussed before, one of the advantages of the proposed converter is its lower current values for the inductor that can easily decrease the dynamic losses and present an efficient converter. This figure shows although the proposed converter has a lower input

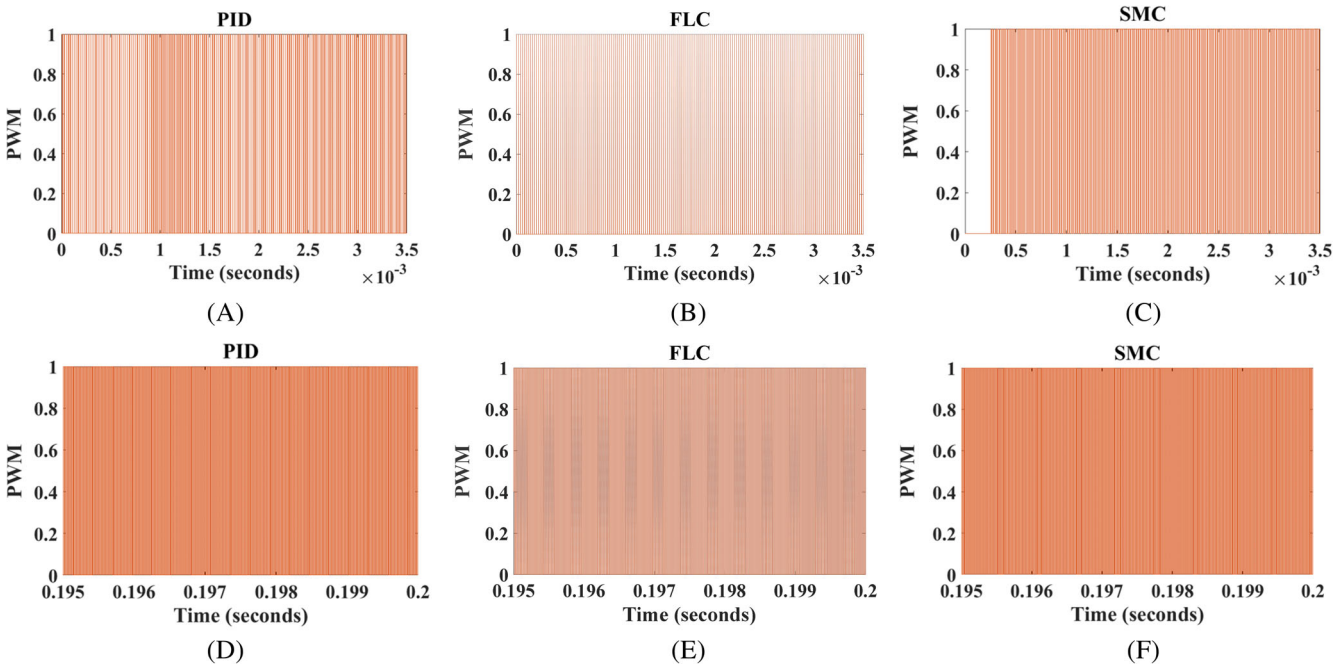

FIGURE 16 Generated PWM signals for the power switch by different controllers

FIGURE 17 A, Input and (B) output currents for the proposed and conventional boost converter

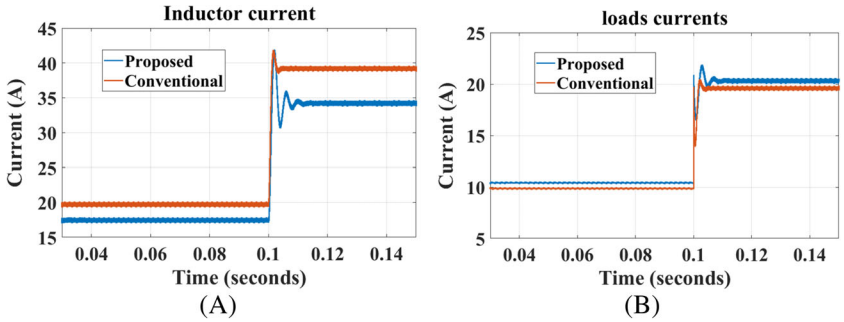

FIGURE 18 A, Output voltage of the boost converter; B, generated pulses by SMC; and C, performance of the controller when the second load acts

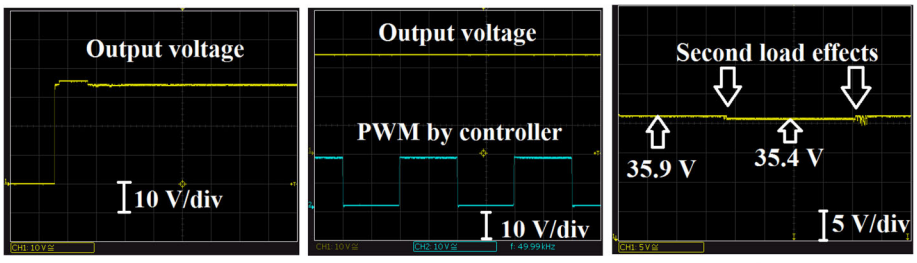

current, it can have a similar current value for the load side with the conventional step-up converter. This result was predictable based on (28) and since the voltage gain of the proposed converter is higher than the conventional boost converter, so with the same output current, it will pass the lower current value in the input side.

To confirm the mathematical and simulation results, a 720 VAh prototype has been implemented. For this purpose, as discussed in theoretical sections, two different e-bikes have been applied to the output ends of the boost converter according to Figure 1B and the performance of the converter and its controller analyzed. For per e-bike, we considered 10 Ah current with a fixed 36 VDC. Figure 18 presents the output voltage of the prototype and shows that the converter can easily generate a fixed 36 VDC. The ripple value of this voltage is around 0.1 V. The overshoot of the voltage at the

start point of the controller is considerable. Very limited value of overshoot or undershoot is seen for this converter. As discussed in mathematical and simulation sections, the switching frequency of the proposed controller is adjusted to 50 KHz. Figure 18B can present this fact and also this figure shows the output voltage of the converter too. Figure 18C illustrates the performance assessment of the controller when the second e-bike enters to the charging station. A 0.5VDC as the drop voltage is reported for the second load. Also, this figure can show the voltage return capability to the primary value when the second load is disconnected.

5 | CONCLUSION

In this study, a PV-based wired type of the e-bike charging station is presented. The proposed converter can be applied in different blocks to generate different values of the DC voltages for various kinds of batteries. Because some of the batteries are charging with 36VDC, and some another with 42 VDC, 48 VDC, 52 VDC, and 54.6 VDC. A DC-DC buck converter is applied between the PV side and boost converter in order to adjust the input voltage of the converter at the 18 VDC and amplify the current values since the most important parameter is current in ECS. A P&O based conventional PI controller has been applied for this block and we focused on the boost side and its controller. A new configuration for the boost converter is considered and the place of the inductors has been changed. The mathematical and simulation results show that this new configuration has a lower amount of the current for the inductor that can directly reduce the dynamic losses of the converter. This is a considerable point because normally the current level of the converter is high at the input and output sides and for to e-bike, it needs to 40 A at the input side and 20 A for the load side. So the dynamic losses can be an important issue in the ECS. The simulation issue is considered for two different topologies based on Figure 1B,C. In the first approach, a block of the proposed converter and controller applied to charge two different e-bikes and for the next stage, an interleaved configuration simulated with two e-bikes for the per block. Results confirm the stability of the converter. Also, all these stages are considered and compared with two PID and FLC control methods and results show better performance for the proposed SMC controller. Finally, a 720 Wh prototype implemented and tested for two e-bikes. For this purpose, at the first stage, the first load and in the next step the second load is added to endpoints of the converter and 0.5 VDC for the voltage drop reported.

LIST OF SYMBOLS AND ABBREVIATIONS

SMC	Sliding Mode Controller
E-bike	electric bicycle
FLC	Fuzzy Logic Controller
RESs	Renewable Energy Sources
EVs	electric vehicles
EMI	Electromagnetic Interface
MPCs	model predictive controllers
CMCs	current mode controllers
ZVT	zero voltage switching
ZCS	zero current switching
ZVT	zero voltage transition
ZCT	zero current transition
DCM	discontinuous current mode
CCM	continuous current mode
I_{SC}	short circuit current (A) for PV cell
$I_{ph,n}$	nominal current
G	irradiation
G_n	nominal irradiation
T	cell temperature (Kelvin)
T_n	cell temperature, nominal state (Kelvin)
K_i	ratio of the short circuit current to the thermal coefficient (A/K)
i_d	diode current (PV cell)
v_d	diode voltage (PV cell)

I_{sat}	diode's reverse saturation current (PV cell)
η	diode's ideal coefficient (PV cell)
V_T	thermal voltage (PV cell)
k_B	Boltzmann constant (J/K)
q	electron charge (Coulomb)
MPPT	maximum power point tracking
P&O	perturbation and observation
V_{in}	input voltages of the boost converter
V_O	output voltages of the boost converter
V_{C1}	voltages on capacitor C_1 (boost converter)
V_{C2}	voltages on capacitor C_2 (boost converter)

ORCID

Davood Ghaderi https://orcid.org/0000-0003-2234-3453

REFERENCES

1. Rydosz A. Amorphous and nanocrystalline magnetron sputtered CuO thin films deposited on low temperature cofired ceramics substrates for gas sensor applications. *IEEE Sen J*. 2014;14(5):1600-1607. https://doi.org/10.1109/JSEN.2014.2301031.
2. Hamed TA, Bressler L. Energy security in Israel and Jordan: the role of renewable energy sources. *Renew Energy*. 2019;135:378-389. https://doi.org/10.1016/j.renene.2018.12.036.
3. Altuntaş EÇ, Turan SL. Awareness of secondary school students about renewable energy sources. *Renew Energy*. 2018;116(Part A):741-748. https://doi.org/10.1016/j.renene.2017.09.034.
4. Patel A, Ferdowsi M. Current sensing for automotive electronics—a survey. *IEEE Trans Veh Technol*. 2009;58(8):4108-4119. https://doi.org/10.1109/TVT.2009.2022081.
5. Brittain JE. Electrical engineering hall of fame: Charles F. Kettering [scanning our past]. *Proc IEEE*. 2009;97(10):1737-1739. https://doi.org/10.1109/JPROC.2009.2027664.
6. Li Z, Khajepour A, Song J. A comprehensive review of the key technologies for pure electric vehicles. *Energy*. 2019;182:824-839. https://doi.org/10.1016/j.energy.2019.06.077.
7. Ahmadi P. Environmental impacts and behavioral drivers of deep de-carbonization for transportation through electric vehicles. *J Clean Prod*. 2019;225:1209-1219. https://doi.org/10.1016/j.jclepro.2019.03.334.
8. Ayyadi S, Bilil H, Maaroufi M. Optimal charging of electric vehicles in residential area. *Sustain Energy Grids Networks*. 2019;19:100240. https://doi.org/10.1016/j.segan.2019.100240.
9. Ezzat M, Dincer I. Exergoeconomic analysis and optimization of a new hybrid fuel cell vehicle. *Int J Hydrogen Energy*. 2019;1-11. https://doi.org/10.1016/j.ijhydene.2019.07.104.
10. Rezaei A, Burl JB, Rezaei M, Zhou B. Catch energy saving opportunity in charge-depletion mode, a real-time controller for plug-in hybrid electric vehicles. *IEEE Trans Veh Technol*. 2018;67(11):11234-11237. https://doi.org/10.1109/TVT.2018.2866569.
11. Xiong R, Zhang Y, Wang J, He H, Peng S, Pecht M. Lithium-ion battery health prognosis based on a real battery management system used in electric vehicles. *IEEE Trans Veh Technol*. 2019;68(5):4110-4121. https://doi.org/10.1109/TVT.2018.2864688.
12. Wild K, Woodward A. Why are cyclists the happiest commuters? Health, pleasure and the e-bike. *J Transp Health*. 2019;14:100569. https://doi.org/10.1016/j.jth.2019.05.008.
13. Chen Z, Kim G-T, Wang Z, et al. 4-V flexible all-solid-state lithium polymer batteries. *Nano Energy*. 2019;64:103986. https://doi.org/10.1016/j.nanoen.2019.103986.
14. Kim SK, Cho KH, Kim JY, Byeon G. Field study on operational performance and economics of lithium-polymer and lead-acid battery systems for consumer load management. *Renew Sustain Energy Rev*. 2019;113:109234. https://doi.org/10.1016/j.rser.2019.06.041.
15. Hannan MA, Hoque MM, Hussain A, Yusof Y, Ker PJ. State-of-the-art and energy management system of Lithium-ion batteries in electric vehicle applications: issues and recommendations. *IEEE Access*. 2018;6:19362-19378. https://doi.org/10.1109/ACCESS.2018.2817655.
16. Iannuzzi D, Rubino L, Di Noia LP, Rubino G, Marino P. Resonant inductive power transfer for an E-bike charging station. *Electr Pow Syst Res*. 2016;140:631-642. https://doi.org/10.1016/j.epsr.2016.05.010.
17. Celentano L, Iannuzzi D, Rubino L. Detailed continuous and discrete–time models and experimental validation to design a power charging station for e-bike clever mobility. *Electr Pow Syst Res*. 2017;147:115-132. https://doi.org/10.1016/j.epsr.2017.01.031.
18. Baek J, Kim J, Lee J, Park M, Moon G. A new standby structure integrated with boost PFC converter for server power supply. *IEEE Trans Power Electron*. 2019;34(6):5283-5293. https://doi.org/10.1109/TPEL.2018.2871138.
19. Veerachary M, Khubchandani V. Analysis, design, and control of switching capacitor based Buck–boost converter. *IEEE Trans Ind Appl*. 2019;55(3):2845-2857. https://doi.org/10.1109/TIA.2018.2889848.
20. Rex SR, Praba DMMSR. Design of PWM with four transistor comparator for DC-DC boost converters. *Microprocess Microsyst*. 2019;1-38. https://doi.org/10.1016/j.micpro.2019.07.003.

21. Mojallizadeh MR, Badamchizadeh MA. Switched linear control of interleaved boost converters. *Int J Elect Power Energy Syst*. 2019;109:526-534. https://doi.org/10.1016/j.ijepes.2019.02.030.
22. Divya Navamani J, Vijayakumar K, Jegatheesan R. Non-isolated high gain DC-DC converter by quadratic boost converter and voltage multiplier cell. *Ain Shams Eng J*. 2018;9(4):1397-1406. https://doi.org/10.1016/j.asej.2016.09.007.
23. Garrigós A, Marroquí D, García A, Blanes JM, Gutiérrez R. Interleaved, switched-inductor, multi-phase, multi-device DC/DC boost converter for non-isolated and high conversion ratio fuel cell applications. *Int J Hydrogen Energy*. 2019;44(25):12783-12792. https://doi.org/10.1016/j.ijhydene.2018.11.094.
24. Alzahrani A, Ferdowsi M, Shamsi P. A family of scalable non-isolated interleaved DC-DC boost converters with voltage multiplier cells. *IEEE Access*. 2019;7:11707-11721. https://doi.org/10.1109/ACCESS.2019.2891625.
25. Knecht O, Bortis D, Kolar JW. ZVS modulation scheme for reduced complexity clamp-switch TCM DC–DC boost converter. *IEEE Trans Power Electron*. 2018;33(5):4204-4214. https://doi.org/10.1109/TPEL.2017.2720729.
26. Abdelhakim A, Mattavelli P, Spiazzi G. Three-phase three-level flying capacitors Split-source inverters: analysis and modulation. *IEEE Trans Ind Electron*. 2017;64(6):4571-4580. https://doi.org/10.1109/TIE.2016.2645501.
27. Khan A, Ben-Brahim L, Gastli A, Benammar M. Review and simulation of leakage current in transformerless microinverters for PV applications. *Renew Sustain Energy Rev*. 2017;74:1240-1256. https://doi.org/10.1016/j.rser.2017.02.053.
28. Rajvikram M, Leoponraj S, Ramkumar S, Akshaya H, Dheeraj A. Experimental investigation on the abasement of operating temperature in solar photovoltaic panel using PCM and aluminium. *Solar Energy*. 2019;188:327-338. https://doi.org/10.1016/j.solener.2019.05.067.
29. Jeyasudha S, Geethalakshmi B. Modeling and analysis of a novel boost derived multilevel hybrid converter. *Energy Procedia*. 2017;117:19-26. https://doi.org/10.1016/j.egypro.2017.05.102.
30. Ramya G, Ganapathy V, Suresh P. Comprehensive analysis of interleaved boost converter with simplified H-bridge multilevel inverter based static synchronous compensator system. *Electr Pow Syst Res*. 2019;176:105936. https://doi.org/10.1016/j.epsr.2019.105936.
31. Prabaharan N, Palanisamy K. Analysis and integration of multilevel inverter configuration with boost converters in a photovoltaic system. *Energ Conver Manage*. 2016;128:327-342. https://doi.org/10.1016/j.enconman.2016.09.088.
32. Mozaffari K, Amirabadi M. A highly reliable and efficient class of single-stage high-frequency AC-link converters. *IEEE Trans Power Electron*. 2019;34(9):8435-8452. https://doi.org/10.1109/TPEL.2018.2888583.
33. Ghaderi D, Celebi M, Minaz MR, Toren M. Efficiency improvement for a DC-DC quadratic power boost converter by applying a switch turn-off lossless snubber structure based on zero voltage switching. *Elektronika Ir Elektrotechnika*. 2018;24(3):15-22. https://doi.org/10.5755/j01.eie.24.3.20977.
34. Li Z, Qian W, Zhang X. An optimized zero-voltage zero-current transition boost converter realized by coupled inductor. *IEEE Trans Power Electron*. 2019;34(9):8882-8893. https://doi.org/10.1109/TPEL.2018.2890132.
35. Mirzaei A, Jusoh A, Salam Z. Design and implementation of high efficiency non-isolated bidirectional zero voltage transition pulse width modulated DC–DC converters. *Energy*. 2012;47(1):358-369. https://doi.org/10.1016/j.energy.2012.09.035.
36. Bao B, Zhang X, Bao H, Wu P, Wu Z, Chen M. Dynamical effects of memristive load on peak current mode buck-boost switching converter. *Chaos Soliton Fract*. 2019;122:69-79. https://doi.org/10.1016/j.chaos.2019.03.003.
37. Fekri M, Molavi N, Adib E, Farzanehfard H. High voltage gain interleaved DC–DC converter with minimum current ripple. *IET Power Electron*. 2017;10(14):1924-1931. https://doi.org/10.1049/iet-pel.2016.0675.
38. Yang L, Liang T, Chen J. Transformerless DC–DC converters with high step-up voltage gain. *IEEE Trans Ind Electron*. 2009;56(8):3144-3152. https://doi.org/10.1109/TIE.2009.2022512.
39. Salvador MA, Lazzarin TB, Coelho RF. High step-up DC–DC converter with active switched-inductor and passive switched-capacitor networks. *IEEE Trans Ind Electron*. 2018;65(7):5644-5654. https://doi.org/10.1109/TIE.2017.2782239.
40. Anzehaee MM, Behnam B, Hajihosseini P. Augmenting ARMarkov-PFC predictive controller with PID-type III to improve boost converter operation. *Control Eng Pract*. 2018;79:65-77. https://doi.org/10.1016/j.conengprac.2018.07.006.
41. Dinniyah FS, Wahab W, Alif M. Simulation of buck-boost converter for solar panels using PID controller. *Energy Procedia*. 2017;115:102-113. https://doi.org/10.1016/j.egypro.2017.05.011.
42. Bayrak G, Ghaderi D. An improved step-up converter with a developed real-timefuzzy-based MPPT controller for PV-based residential applications. *Int Trans Electr Energ Syst*. 2019;29:e12140. https://doi.org/10.1002/2050-7038.12140.
43. Ozdemir S, Altin N, Sefa I. Fuzzy logic based MPPT controller for high conversion ratio quadratic boost converter. *Int J Hydrogen Energy*. 2017;42(28):17748-17759. https://doi.org/10.1016/j.ijhydene.2017.02.191.
44. Cunha RBA, Inomoto RS, Altuna JAT, Costa FF, Di Santo SG, Sguarezi Filho AJ. Constant switching frequency finite control set model predictive control applied to the boost converter of a photovoltaic system. *Solar Energy*. 2019;189:57-66. https://doi.org/10.1016/j.solener.2019.07.021.
45. Xiao Z, Ren J, Xu Y, et al. An automatic slope compensation adjustment technique for peak-current mode DC-DC converters. *AEU Int J Electron Commun*. 2019;110:152860. https://doi.org/10.1016/j.aeue.2019.152860.
46. Wen Y, Rose M, Fernandes R, Van Otten R, Bergveld HJ, Trescases O. A dual-mode driver IC with monolithic negative drive-voltage capability and digital current-mode controller for depletion-mode GaN HEMT. *IEEE Trans Power Electron*. 2017;32(1):423-432. https://doi.org/10.1109/TPEL.2016.2537002.
47. Kumar KR. Implementation of sliding mode controller plus proportional double integral controller for negative output elementary boost converter. *Alex Eng J*. 2016;55(2):1429-1445. https://doi.org/10.1016/j.aej.2016.03.027.

48. Repecho V, Biel D, Olm JM, Fossas E. Robust sliding mode control of a DC/DC boost converter with switching frequency regulation. *J Franklin Inst*. 2018;355(13):5367-5383. https://doi.org/10.1016/j.jfranklin.2018.05.028.
49. Chincholkar SH, Jiang W, Chan C. An improved PWM-based sliding-mode controller for a DC–DC Cascade boost converter. *IEEE Trans Circuits Syst II: Exp Briefs*. 2018;65(11):1639-1643. https://doi.org/10.1109/TCSII.2017.2754292.
50. Chincholkar SH, Chan C. Design of fixed-frequency pulsewidth-modulation-based sliding-mode controllers for the quadratic boost converter. *IEEE Trans Circuits Syst II: Exp Briefs*. 2017;64(1):51-55. https://doi.org/10.1109/TCSII.2016.2546902.
51. Ardashir JF, Sabahi M, Hosseini SH, Blaabjerg F, Babaei E, Gharehpetian GB. A single-phase transformerless inverter with charge pump circuit concept for grid-tied PV applications. *IEEE Trans Ind Electron*. 2017;64(7):5403-5415. https://doi.org/10.1109/TIE.2016.2645162.
52. Kan S, Ruan X, Dang H, Zhang L, Huang X. Second harmonic current reduction in front-end DC—DC converter for two-stage single-phase photovoltaic grid-connected inverter. *IEEE Trans Power Electron*. 2019;34(7):6399-6410. https://doi.org/10.1109/TPEL.2018.2877590.
53. M. Lotfi Nejad, B. Poorali, E. Adib and A. A. Motie Birjandi, "New cascade boost converter with reduced losses," *IET Power Electron*, vol. 9, no. 6, pp. 1213–1219, 18, 2016. doi: https://doi.org/10.1049/iet-pel.2015.0240.
54. Ghaderi D, Bayrak G. A novel step-up power converter configuration for solar energy application. *Elektronika Ir Elektrotechnika*. 2019;25(3):240-250. https://doi.org/10.5755/j01.eie.25.3.23676.
55. Wu H, He X. Single phase three-level power factor correction circuit with passive lossless snubber. *IEEE Trans Power Electron*. 2002;17(6):946-953. https://doi.org/10.1109/TPEL.2002.805578.

How to cite this article: Huang R, Hong F, Ghaderi D. Sliding mode controller-based e-bike charging station for photovoltaic applications. *Int Trans Electr Energ Syst*. 2020;30:e12300. https://doi.org/10.1002/2050-7038.12300